A Glycyl Radical Site in the Crystal Structure of a Class III Ribonucleotide Reductase

Derek T. Logan,[1]* Jessica Andersson,[2] Britt-Marie Sjöberg,[2] Pär Nordlund[1]*

Ribonucleotide reductases catalyze the reduction of ribonucleotides to deoxyribonucleotides. Three classes have been identified, all using free-radical chemistry but based on different cofactors. Classes I and II have been shown to be evolutionarily related, whereas the origin of anaerobic class III has remained elusive. The structure of a class III enzyme suggests a common origin for the three classes but shows differences in the active site that can be understood on the basis of the radical-initiation system and source of reductive electrons, as well as a unique protein glycyl radical site. A possible evolutionary relationship between early deoxyribonucleotide metabolism and primary anaerobic metabolism is suggested.

Ribonucleotide reductases (RNRs) are essential enzymes for all life, constituting the only de novo catalytic path for the production of the deoxyribonucleotides required for DNA synthesis. The chemically very difficult replacement of the ribose 2′-OH in ribonucleotides by hydrogen is made possible through the use of free-radical chemistry. The presently characterized RNRs can be divided into three classes on the basis of their primary structure and, more importantly, their radical generation mechanism (*1*). Class I RNRs are composed of two dimeric subunits, R1 and R2. They generate a stable tyrosyl free radical on the R2 subunit through activation of molecular O_2 by a dinuclear iron center. This radical is most likely transferred over a long hydrogen-bonded radical transfer pathway to the active site on the R1 subunit (*2*, *3*). Class II enzymes are monomers or homodimers and use adenosylcobalamin to generate transient 5′-deoxyadenosine and cysteine radicals (*4*).

Class III RNRs are expressed by certain strictly or facultatively anaerobic bacteria under anaerobic conditions (*5*). They have quaternary structure $\alpha_2\beta_2$ (*6*, *7*). The active site and allosteric regulatory sites lie in the large α_2 subunit (gene product NrdD, molecular size in phage T4 136 kD, 2 × 605 amino acids), whereas the small β_2 subunit, also known as the activase (NrdG, molecular size in T4 36 kD, 2 × 156 amino acids), carries out homolytic cleavage of *S*-adenosylmethionine (AdoMet) in association with an iron-sulfur cluster to generate the stable glycyl radical near the COOH-terminus of NrdD, at residue 580 (*7*–*9*). Exposure of the active complex to oxygen results in inactivation by cleavage adjacent to the glycyl radical and loss of the COOH-terminal 25 residues (*10*). In class I and II reductases the original radical is transferred to a thiyl radical in the active site (*4*, *11*), and this is also believed to be the case for class III. The reducing equivalents for reduction of the ribonucleotide in class I and II are delivered from thioredoxin or glutaredoxin and are shuttled to the active site by way of two Cys residues in the COOH-terminus of the large subunit (*3*, *12*). In class III reductases, formate serves as the overall reductant (*13*), being oxidized to CO_2. Class III RNRs have no significant overall sequence similarity to class I or II enzymes in the putative active-site domain, but sequence homology in a nucleotide-binding regulatory domain present in some RNRs, combined with similarities in allosteric behavior and radical chemistry (*1*, *5*), have been used to argue for a common evolutionary origin for the three classes.

The concept of an RNA world preceding the DNA world of today is based on the versatility of the RNA molecule for both storage of genetic information and as a catalyst. Supporting the RNA world hypothesis is the existence of metabolic paths for de novo synthesis of RNA precursors, whereas DNA precursors are only produced through reduction of ribonucleotides by RNR. Making the reasonable assumption that an autotrophic production of deoxyribonucleotides was present at an early stage of the DNA world, an understanding of the evolutionary relationships between the various RNR families

[1]Department of Biochemistry and [2]Department of Molecular Biology, Stockholm University, S-106 91 Stockholm, Sweden.

*To whom correspondence should be addressed. E-mail: derek@biokemi.su.se, par@milvus.biokemi.su.se

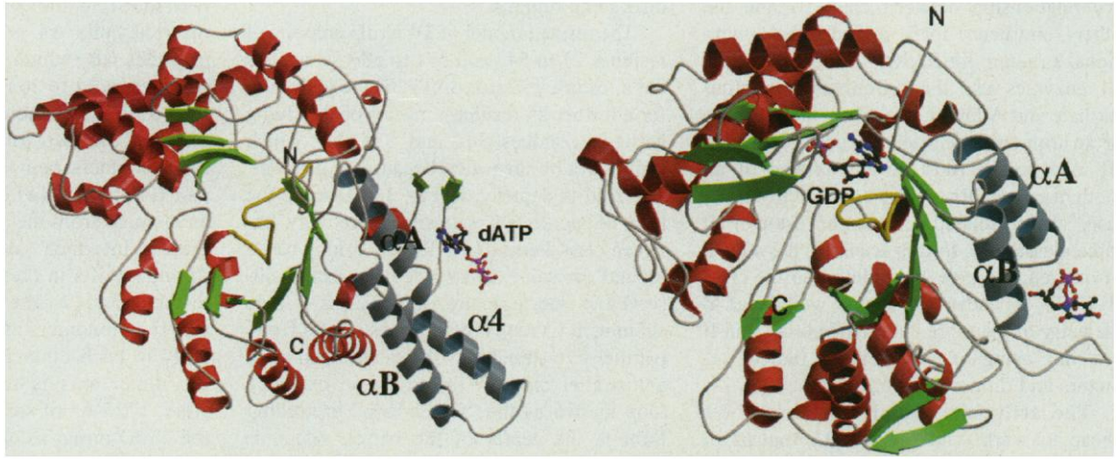

Fig. 1. A comparison of the folds of the active-site domains of class I RNR (R1) and class III RNR (NrdD) (*15*). β strands are colored green, α helices are red (except where noted), and loops are white. Only one monomer of each dimer is shown. (Left) NrdD. The allosteric effector molecule dATP is shown in a ball-and-stick representation. The "finger loop" is drawn as a yellow coil. The lengthened helices αA and αB, and the inserted helix α4, at the dimer interface, are colored light blue. For clarity, the COOH-terminal region after the end of the last β strand is not shown. (Right) R1. Only the β-barrel domain is depicted (residues 225 to 734). The substrate GDP is depicted in the center of the barrel and the allosteric effector dTTP at the edge (*20*), as ball-and-stick models. Helices αA and αB, which form a four-helix bundle at the dimer interface, are shown in light blue.

Table 1. Data collection and processing statistics. A first native data set was collected at the Swiss-Norwegian beamline of the European Synchrotron Radiation Facility to 3.0 Å. A higher resolution data set extending to 2.75 Å was later obtained at beamline X12B of the NSLS from a fresher crystal soaked in 4 mM dATP and 4 mM CTP for 2 days. Data were integrated and merged with the HKL package (*46*), and further data analysis was performed with programs from the CCP4 package (*47*). For details of the structure solution and refinement, see (*48*).

	Native	+dATP/CTP	MMA			K_2OsO_4		$IrCl_3$
Synchrotron station	ESRF SNBL	NSLS X12B	DESY X11	ESRF BM14		ESRF BM14		NSLS X12B
Diffraction limits (Å)	3.0	2.75	3.65	3.5	3.5	3.4	3.3	3.4
λ (Å)	0.873	1.0714	0.9096	1.0089	0.9528	1.1394	1.1271	0.949
$R_{merge}(I)$* (%)	7.9/ 39.4†	9.0/ 35.8†	8.7/ 7.9‡	7.8/ 4.0‡	8.9/ 8.2‡	5.9/ 3.6‡	6.8/ 4.3‡	9.1/ 7.4‡
Completeness (%)	94.9/ 93.4†	92.1/ 69.6†	81.6/ 69.4‡	96.3/ 94.9‡	96.5/ 95.0‡	96.7/ 83.6‡	97.9/ 76.6‡	93.6/ 61.8‡
Multiplicity of observation	4.4	2.7	3.3	6.3	4.9	6.2	3.8	2.8
No. of sites			7	7		5		3
Phasing power				1.60		1.92		0.7
R_{cullis}§			–/ 0.95‡	0.71/ 0.92‡	–/ 0.95‡	0.67/ 0.90‡	–/ 0.96‡	0.90/ 0.97‡

*$R_{merge}(I) = \Sigma_{j,k} |I_{j,k} - \langle I \rangle_j| / \Sigma_{j,k} I_{j,k}$, where $I_{j,k}$ are the k individual observations of each reflection j and $\langle I \rangle_j$ is the value after weighted averaging. †These figures refer to the highest resolution shell (3.05 to 3.00 Å for native, 2.80 to 2.75 Å for dATP/CTP). ‡The second figure refers to the relevant statistic for Friedel mates/anomalous contribution. Synchrotron beamlines: Swiss-Norwegian Beamline (SNBL), European Synchrotron Radiation Facility (ESRF, Grenoble, France); station X12B, National Synchrotron Light Source (NSLS, Brookhaven National Laboratory, NY, USA); station X11, European Molecular Biology Laboratory (EMBL) outstation, DESY, Hamburg; station BM14, ESRF. Other abbreviations: MMA, methylmercury acetate; KOs, potassium osmate; IrCl, iridium chloride; ND, not determined. §$R_{cullis} = \Sigma \varepsilon_{iso} / \Sigma \Delta_{iso}$ for acentric reflections and $\Sigma \varepsilon_{ano} / \Sigma \Delta_{Bijvoet}$ for anomalous differences, where ε_{iso} and ε_{ano} are the isomorphous and anomalous lack of closure respectively, and Δ_{iso} is the isomorphous difference and $\Delta_{Bijvoet}$ is the Bijvoet difference.

Table 2. Statistics for refinement of the NrdD model. The two values given for number of reflections represent the working and free sets, respectively. An acceptable percentage of the residues in structure native 1 (76.6%) and of those in structure native 2 (79.7%) lie in the core regions of the Ramachandran plot as defined in (*49*).

	Native	+dATP/CTP
Resolution range (Å)	15–3.0	30–2.75
No. of reflections	21496/2108	29676/2512
R_{model} (%)	26.4	23.0
R_{free} (%)	33.8	30.5
No. of atoms	4100	4370
rms deviations from ideal geometry		
Bonds (Å)	0.017	0.009
Angles (°)	4.0	1.6
Torsion angles (°)	21.0	25.9

could give essential information on the nature of the transition between the RNA and DNA worlds. Several lines of evidence point to an evolutionary kinship between class I and class II RNRs: conservation of five essential Cys residues (*3*, *14*, *15*), participation of a thiyl radical in the reaction (*4*, *11*), and a significant level of overall sequence homology between class I and recently determined class II sequences from Archaea and deeply rooted Eubacteria (*16*). However, no strong evidence has been available for an evolutionary relationship between class III and the others, and hence for a unified three-dimensional structure for RNRs. The fact that class III enzymes use the primitive metabolites formate and AdoMet, as well as the presence of an iron-sulfur cluster, suggests that class III may be the most closely related of all modern-day RNRs to the so-called "ur-reductase," the postulated common ancestor of all three classes (*1*). In this scenario, the advent of oxygen on Earth, being lethal to the class III RNR–dependent organisms, would lead to the entry of the more "modern" class I and II systems, using oxygen-resistant radical cofactors and dithiol reduction chemistry.

The active-site fold is conserved. We chose to work with the G580A mutant of NrdD in order to avoid the O_2-dependent cleavage associated with the native enzyme and thus allow purification and crystallization of the intact complex under aerobic conditions (*17*). The structure was solved by a combination of multiple isomorphous replacement and multiple wavelength anomalous dispersion methods, with three derivatives (Table 1). Refinement was continued with a higher resolution data set obtained from a crystal soaked in deoxyadenosine 5′-triphosphate (dATP) and cytidine 5′-triphosphate (CTP). The current refined model has an R factor of 23.0% and R_{free} of 30.5%, with good geometry (Table 2). The relatively high R factors are due to the presence of several disordered regions.

The refined model of T4 NrdD consists of residues 27 to 542 and 571 to 586, as well as the allosteric effector dATP. There is density for a further 25 residues, most probably lying between residues 542 and 571, but which cannot yet be identified because of disorder. The fold is depicted in Fig. 1A. Despite the lack of significant sequence homology between class I and III RNRs, the fold is based around the same 10-stranded β/α barrel observed in the structure of the class I large subunit, R1 (*15*) (Fig. 1), consisting of two parallel five-stranded β sheets arranged in an antiparallel manner, linked by an extended loop known as the "finger loop" protruding through the center of the barrel, which is flanked on the outside by helices. 163 Cα atoms from the barrel cores (31% of NrdD) can be superimposed with a root-mean-square deviation of 1.5 Å (*18*). In view of the mechanistic and sequence similarities between classes I and II outlined above, we can therefore anticipate that all three classes, despite their substantially different cofactors and quaternary structures, will have the same active-site fold and likely be of common evolutionary origin (*19*).

The major differences in topology between NrdD and R1 lie at the dimer interface, in particular between β strands B and C, which represents part of the substrate specificity allosteric site in both enzymes. Structural changes induced by deoxynucleoside triphosphate (dNTP) binding at this site have been suggested to mediate substrate specificity on the neighboring monomer through interaction of loops across the dimer interface (*20*). In R1, the dimer-stabilizing interactions come mainly from a short four-helix bundle consisting of helices A and B from each subunit. In NrdD, two long helices, α4 and αB, replace the simple crossover helix αB of the repeated β-α motif in the R1 barrel (Fig. 1). The inserted helix α4 is 22 residues long and precedes αB, which is lengthened from 12 residues in R1 to 26 in NrdD (Fig. 1). These long antiparallel helices pack against each other at the two-fold axis (Fig. 2A), the main contacts being made by the parallel pair α4 and α4′ (where the prime indicates an element from the second monomer). The dimer interface is greatly remodeled through shifts in these helices with respect to the strands of the barrel (Fig. 2C), such that the monomers are oriented very differently to each other in NrdD. In particular, the dimer axis is rotated by almost 90°. Also, 1725 Å^2 of surface area are buried in the NrdD dimer as opposed to only 744 Å^2 in R1 (*21*).

The class III active site. Figure 3A shows the active site of NrdD with modeled guanosine 5′-diphosphate (GDP), obtained

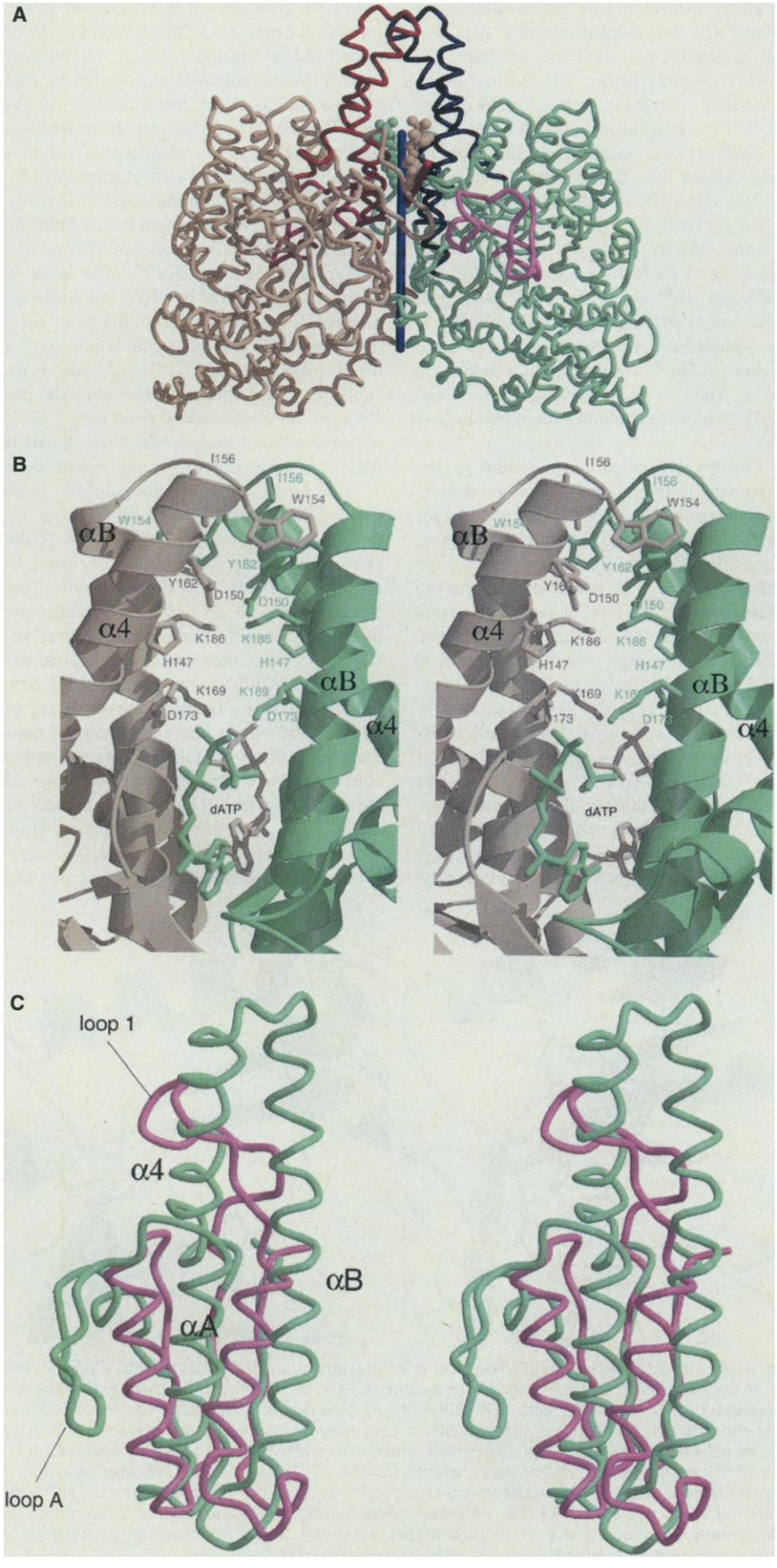

Fig. 2. Altered dimer interfaces of NrdD caused by insertion and elongation of helices and loops with respect to R1. (**A**) Dimer interactions in NrdD. The view is perpendicular to the two-fold axis, which is shown as a blue vertical rod. The dimer axis in R1 is shown for comparison, as a red rod approximately perpendicular to the page. Monomer 1 is drawn in beige, monomer 2 in aquamarine. Helices αA, α4, and αB are drawn in rust and dark blue for monomers 1 and 2, respectively. The COOH-terminal loop and partially disordered area are drawn in shades of purple. The COOH-terminal loop of the left-hand monomer is mostly hidden, on the rear of this view. The allosteric effector dATP is represented as a CPK model, in the same colors as the respective monomers. (**B**) Close-up stereo view of the helix interactions at the dimer interface. The helices are anchored at the top by a hydrophobic cluster consisting of residues Trp^{154}, Ile^{156}, and Tyr^{162} of each monomer. In contrast, the middle portions of the helices contain many basic residues that protrude into a putative solvent-filled channel. Other secondary-structure elements involved in dimer-forming interactions closer to the body of the barrels are loops 90 to 100, 185 to 192, 221 to 228, and the NH_2-terminal helix α1, on the bottom of the dimer as seen in (A). (**C**) A large shift in the orientation of the dimer-forming helices relative to the three strands of the β barrel to which they are connected. This shift, together with the lengthening and insertion of helices, is primarily responsible for the almost 90° rotation of the dimer axis with respect to R1. The molecules are oriented to best superpose strands A to C of the barrel (seen from left to right). Residues from R1 are drawn in purple, from NrdD in aquamarine.

by superimposing the coordinates of R1 with bound GDP (*20*) on NrdD. Residues in the vicinity of GDP that are conserved in all known NrdD sequences are depicted, as well as potentially relevant, nonconserved residues. The substrate of class III reductases are NTPs, but we have conservatively chosen not to model the third phosphate here.

A reaction mechanism for RNRs has been proposed that could be general at least for classes I and II (*22*) and that is given weight by functional and structural (*20*) studies [for a recent discussion see (*23*)]. In class I RNRs, three conserved cysteine residues in the active site are essential for activity (*24*). Cys^{439} (*Escherichia coli* numbering) lies at the end of a loop that penetrates through the center of the barrel, and is suggested to be responsible for abstraction of a H atom from C3′ of the substrate ribose to initiate reduction (*25*) (Fig. 3B). Cys^{225} and Cys^{462} lie in close proximity, at equivalent positions on strands βA and βF in opposite halves of the barrel (*15*), and deliver two reducing equivalents to the substrate, being thereby oxidized to a disulfide (Fig. 3B). Only two of these essential Cys residues are conserved in class III, namely Cys^{290} (equivalent to Cys^{439} in R1) at the tip of the loop and Cys^{79} (equivalent to Cys^{225}) on strand βA. The location of Cys^{290} in the active site is consistent with results obtained from [γ-^{32}P]8-N_3ATP labeling (*26*). In place of the third Cys (Cys^{462} in R1) is found Asn^{311}, conserved in all NrdD sequences. Because disulfide bond formation is a critical step in the proposed reaction mechanism (*20*, *22*), it is clear that it cannot be general for all classes. However, the sequential reactivation process in class I and II RNRs, in which reduction of the active-site disulfide by a Cys pair near the COOH-terminus is followed by reduction of the COOH-terminal disulfide by thioredoxin or glutaredoxin (*12*, *15*), is not necessary in NrdD, whose overall reductant is formate (*13*). On the basis of the current structure, the most plausible suggestion is that formate binds directly in the active site, where it would be well placed to pass reducing equivalents through Cys^{79} (*27*).

Two further important side chains in class I RNRs are absent in NrdD (Fig. 3). Glu^{441} (*E. coli* R1 numbering) is suggested to participate in base-catalyzed elimination of a water molecule across the C2′-C3′ bond to remove the 2′-OH group. This is supported by structural studies (*20*), site-directed mutagenesis (*28*), chemical studies with substrate analogs (*29*), and quantum mechanical calculations (*30*). Asn^{437} has been suggested to participate in a hydrogen-bonded chain important in the latter stages of reduction (*20*). Asn^{437} and Glu^{441} are replaced in the NrdD sequence by Met^{288} and Ser^{292}, neither of which have their side chains oriented to interact with the modeled substrate. Arg^{291} is also directed away from the substrate. No suitably oriented acidic side chain can be found in the active site to take on the role of Glu^{441} (*31*). It is possible that formate plays the dual role of proton donor or shuttle in the early stages of the reaction (replacing Glu^{441}), and hydrogen donor at a later step (replacing Cys^{462}) (*32*).

Other strictly conserved residues in the active site of T4 NrdD are shown in Fig. 3A. His^{64} and His^{66} almost certainly participate in phosphate binding, the former probably to the γ-phosphate. The base is likely to stack on top of Phe^{194}, which in turn stacks on Phe^{231}. The lack of a side chain at Gly^{125} and Gly^{126} is important to make room for the base (*20*).

The glycyl radical is proximal to the active site. In the initial 3 Å electron density maps, it was not possible to build a model for the COOH-terminal 65 residues. However, data collected from fresher crystals soaked with dATP and CTP revealed clear density for residues 571 to 586 (Fig. 4A). These form a long loop directed into the barrel, of which the tip, containing the mutated glycyl radical site Ala^{580}, meets the tip of the "finger loop" in the active site (Fig. 4B). This places Ala^{580} surprisingly close to Cys^{290}, the putative radical cysteine. The distance between Cα of Ala^{580} and Sγ of Cys^{290} is only 5.2 Å. This suggests that a radical could be generated on Cys^{290} in the native enzyme through short-range transfer of a H atom to Gly^{580}, in contrast to class I, where the stable tyrosyl radical is generated at a buried site in the separate R2 protein and transferred by way of a long radical transfer pathway involving at least six amino acid side chains. Taking into account the possible steric effects of the Gly^{580}→Ala mutation, direct abstraction is a likely possibility, but neighboring residues may also participate in radical transfer (*33*).

The conformation around Ala^{580} is partly determined by two hydrogen bonds from the main chain nitrogens of residues 580 and 581 to the side chain of Glu^{446}. The latter is completely conserved in all known NrdD sequences. It lies at the NH_2-terminus of helix αH, which in R1 hydrogen bonds to the α-phosphate of the GDP substrate (*20*). Glu^{446} may participate in fine-tuning the position of the glycyl radical relative to Cys^{290} in response to substrate binding, which would thus act as a trigger for Cys radical formation.

The NrdG subunit and AdoMet most likely bind on the outside of the loop, on the other side of Glu^{446} (Fig. 4B). If the conformation of native NrdD is the same as that seen in the G580A mutant, both of the H atom positions on Gly^{580} would be relatively inaccessible for direct H atom abstraction by a 5′-deoxyadenosyl radical derived from AdoMet, because of steric hindrance caused by the hydrogen bonding of Glu^{446} to the main chain nitrogens of residues 580 and 581. This suggests that some conformational change occurs before H atom abstraction. The buried nature of Gly^{580} is in agreement with the very slow solvent exchange observed in D_2O (*7*, *34*). More structural and spectroscopic studies

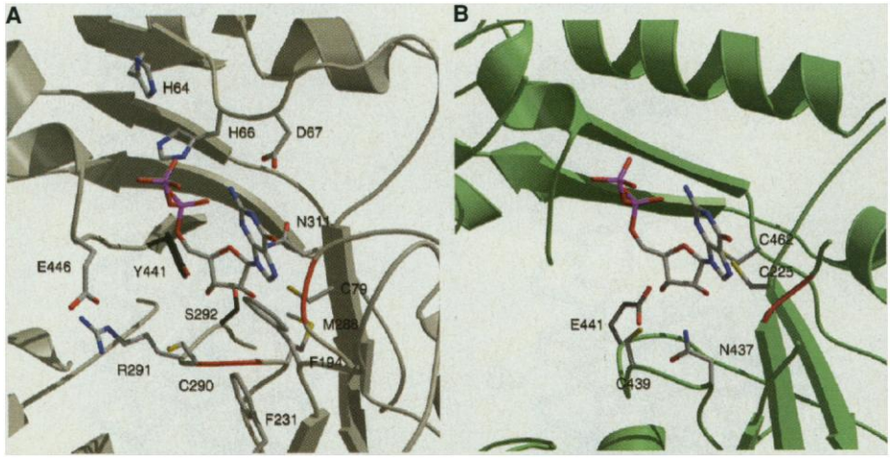

Fig. 3. (**A**) The active site of NrdD. The view is looking down into the β barrel, with Cys^{290} at the tip of the finger loop. In the center of the picture is GDP, as modeled by superimposing the Cα coordinates of R1 in complex with GDP (*20*) on NrdD. Side chains of all strictly conserved residues near the putative NTP-binding site and others that may be of importance are shown. Strictly conserved residues are drawn with light gray C atoms. The widely, but not totally, conserved Tyr^{441} and Ser^{292} are drawn with darker gray C atoms. Conserved Gly residues are indicated by coloring the coil regions red. The upper stretch contains Gly^{124} and Gly^{125}, the lower stretch Gly^{289}. (**B**) Sketch of the active site of R1, for comparison. Functionally important residues as identified by mutagenesis, and theoretical and structural studies, are drawn. Gly^{253}, important in providing space for the substrate base moiety, is drawn as a short stretch of red coil.

are needed on the NrdG subunit and its interactions with AdoMet.

The small-subunit NrdG remains elusive. The (4Fe-4S) cluster that interacts with AdoMet to generate Gly^{580} is formed only in dimeric NrdG (*9*). We observe no NrdG in crystals of the complex (*35*). Assuming coaxial aligment of dimeric NrdD and NrdG, the most plausible position for NrdG is on the lower face of NrdD as seen in Fig. 2A. The distance between symmetry-equivalent Gly^{580} residues in the dimer is ~50 Å, which makes it difficult to imagine how a single iron-sulfur cluster positioned on the dimer axis could generate a 5′-deoxyadenosyl radical that would then abstract a H atom from Gly^{580}, because the distance to the (4Fe-4S) cluster would be about 20 Å. It seems likely that two CxxC motifs, disordered in the present structure, preceding the Gly radical site (residues 543 to 546 and 561 to 564, respectively) are part of a structural motif involved in radical generation. Mutagenesis of any of these cysteines to Ser results in lack of glycyl radical–dependent cleavage in the presence of oxygen (*36*).

Hints of an evolutionary relationship to other glycyl radical enzymes. Despite very limited sequence homology, NrdD intriguingly shares many of its radical-generation properties with pyruvate formate lyase (PFL), an enzyme involved in anaerobic fermentation (*37*). The latter is also a large dimeric protein with a glycyl radical near the COOH-terminus (*38*). This radical is generated by direct abstraction of the Pro-S hydrogen of the glycine by a 5′-deoxyadenosyl radical produced through cleavage of AdoMet by a small iron-sulfur protein (*39*) with high homology to NrdG (*3*). However, the activase is monomeric, rather than dimeric as in class III RNRs (*40*). The residues immediately surrounding the glycyl radical site in PFL are highly homologous to NrdD (*41*), and the product of the PFL reaction, formate, is the overall reductant of NrdD. These similarities raise the question whether they could be evolutionarily related. In addition, two further short regions of sequence homology are observed (Fig. 4C) (*3*).

The NrdD structure suggests a role for these conserved residues. Asp^{268}, at the beginning of strand βE, makes a salt bridge to Arg^{577} which also appears to be essential for loop stabilization (*42*). The side chain of Met^{265} provides a buttressing interaction between the last strand of the β barrel, βJ, and the extended portions of the COOH-terminal loop (Fig. 4D). It participates in a hydrophobic cluster involving Val^{540}, Ile^{575}, and Leu^{582}, which are hydrophobic in all NrdD and PFL sequences. This suggests a distant but significant structural homology between NrdD and PFL. Electron paramagnetic resonance spectroscopy of PFL inactivated by substrate analogs and dioxygen (*43*) has suggested that in PFL the Gly and Cys radicals are in rapid exchange and lie spatially close to each other, which is consistent with the structure of the Gly-Cys radical site in NrdD. The methyl group of Ala^{580} in NrdD replaces the Pro-S hydrogen of Gly^{580} in the native enzyme and faces toward the surface. If we assume a similar structure for PFL, this may also explain why this proton is stereospecifically removed in PFL (*44*). PFL also provides an alternative model for NrdD-NrdG

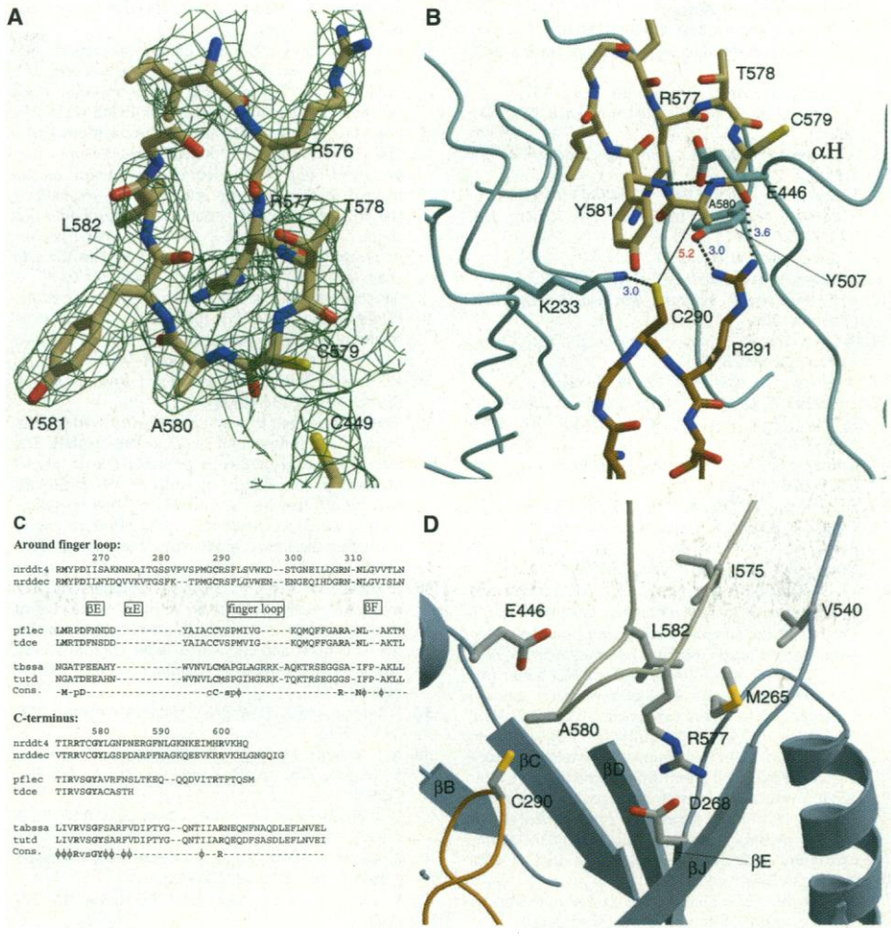

Fig. 4. **(A)** The glycyl radical site in the COOH-terminal region of NrdD. Electron density for the COOH-terminal loop, which extends into the top of the barrel toward the active site. Also drawn is Cys^{449}. The Sγ atoms of Cys^{449} and Cys^{579} lie at a distance of 4.0 Å from each other. The figure shows the beginning of a break in the electron density between them that may be due to a covalent modification. The map has coefficients $|F_o| - |F_c|$ and is calculated after removal of the displayed atoms from the phasing model, application of small random shifts to the atoms, and conjugate gradient energy minimization. The contour level is 3σ. **(B)** Conformation of the COOH-terminal loop and its interactions with the body of NrdD. The loop is colored beige and the rest of the protein light blue. The finger loop extends up from the bottom of the figure and is colored brown. Possibly significant hydrogen bonds are indicated; the bond between Arg^{291} and Cys^{579} is rather long, at 3.6 Å, but could be significant within the experimental coordinate error at this resolution. **(C)** Sequence alignment of the sequence preceding the finger loop and of the COOH-terminal region in NrdD and PFL. Only two representative NrdD sequences and one PFL sequence are shown. nrddt4, bacteriophage T4 NrdD (SwissProt P07071); nrddec, *E. coli* NrdD (P28903); pflec, *E. coli* PFL (P09373); tbssa, benzylsuccinate synthase from *Thauera aromatica* (GenBank 3184131); tutd: TutD protein from *T. aromatica* (independently identified, also a benzylsuccinate synthase; GenBank 3127057); tdce, bifunctional PFL/2-ketobutyrate formate lyase from *E. coli* (P42632). Key to consensus sequence (cons.): bold letters represent residues conserved in more than 80% of known sequences, lowercase letters represent conservation in more than half the sequences; ϕ, hydrophobic; (+) positively charged. **(D)** Anchoring of the COOH-terminal loop by interactions that suggest an evolutionary relationship to pyruvate formate lyase and other glycyl radical–containing enzymes. The color scheme is the same as that in (B). The residues Arg^{577}, Met^{265}, and Asp^{268} are conserved in all NrdD sequences and in all but one of the PFL sequences.

interaction. A NrdG dimer could interact "end-on" with one of the NrdD monomers in such a way that the (4Fe-4S) cluster approaches the glycyl radical site, similar to the interaction, although transient, of monomeric PFL activase with the PFL dimer (*40*).

Recent results have shown that NrdD and PFL belong to a growing family of glycyl radical enzymes, which now contains members involved in toluene metabolism and threonine degradation (*45*). Arg^{577} is also conserved in these systems (Fig. 4D). It may thus be that the structure of NrdD represents a common framework for the whole family. Asn^{311} is also conserved in PFL, which binds pyruvate, but not in the enzymes where a carboxylate moiety is not involved, raising the possibility that it is part of a common carboxylate binding site. An evolutionary link to PFL, a likely participant in early pre-aerobic glycolysis, raises the possibility of a progression from a potent radical-based catalytic machinery in primary metabolism to the first system performing the difficult reduction of the 2′ carbon-oxygen bond of ribonucleotides.

References and Notes

1. P. Reichard, *Science* **260**, 1773 (1993).
2. P. Nordlund, B.-M. Sjöberg, H. Eklund, *Nature* **345**, 593 (1990).
3. B.-M. Sjöberg, *Struct. Bonding* **88**, 139 (1997).
4. S. Licht, G. J. Gerfen, J. Stubbe, *Science* **271**, 477 (1996).
5. A. Jordan and P. Reichard, *Annu. Rev. Biochem.* **67**, 71 (1998).
6. X. Sun *et al.*, *J. Biol. Chem.* **270**, 2443 (1995).
7. P. Young, J. Andersson, M. Sahlin, B. M. Sjöberg, *ibid.* **271**, 20770 (1996).
8. X. Sun *et al.*, *ibid.* , p. 6827.
9. S. Ollagnier *et al.*, *ibid.* **272**, 24216 (1997).
10. D. S. King and P. Reichard, *Biochem. Biophys. Res. Commun.* **206**, 731 (1995).
11. A. L. Persson, M. Sahlin, B.-M. Sjöberg, *J. Biol. Chem.* **273**, 31016 (1998).
12. A. Åberg *et al.*, *ibid.* **264**, 12249 (1989).
13. E. Mulliez, S. Ollagnier, M. Fontecave, R. Eliasson, P. Reichard, *Proc. Natl. Acad. Sci. U.S.A.* **92**, 8759 (1995).
14. S. Booker, S. Licht, J. Broderick, J. Stubbe, *Biochemistry* **33**, 12676 (1994).
15. U. Uhlin and H. Eklund, *Nature* **370**, 533 (1994).
16. J. Riera, F. T. Robb, R. Weiss, M. Fontecave, *Proc. Natl. Acad. Sci. U.S.A.* **94**, 475 (1997); A. Tauer and S. Benner, *ibid.*, p. 53; A. Jordan *et al.*, *ibid.*, p. 13487.
17. T4 NrdD(G580A) and NrdG were coexpressed and copurified as described, with minor modifications (7). Crystals of the complex were grown by the hanging drop vapor diffusion method. Two microliters of protein (20 to 30 mg/ml) in 20 mM tris-HCl buffer (pH 8.5) were mixed with 2 μl of a reservoir solution containing 28 to 32% polyethylene glycol (PEG 400), 0.25 M $MgCl_2$, 0.1 M Hepes buffer (pH 7.5), and 5 mM dithiothreitol (DTT). Bipyramidal crystals grew to a maximum size of 0.5 mm from point to point after about 3 weeks. The crystals belonged to space group $P4_32_12$ with unit cell dimensions $a = b = 98.2$ Å, $c = 244.0$ Å. Assuming one αβ monomer in the asymmetric unit, one obtains a solvent content of 64% and $V_m = 3.4$ Å^3 per dalton.
18. Superposition of structures was carried out with the SHP program (D. I. Stuart, unpublished data).
19. The T4 enzyme does not present us with a model for the NH_2-terminal domain present in some other NrdD sequences, which corresponds to the overall activity allosteric site domain in R1. However, conservation of essential nucleotide recognition residues in NrdD sequences where the domain is present suggests that it will have a very similar structure to that seen in R1.
20. M. Eriksson *et al.*, *Structure* **5**, 1077 (1997).
21. The altered dimer interface makes it impossible for dNTPs to bind as they do in R1. dATP binds in a cleft between αA of one monomer and αB of monomer 2, and makes contacts to the hairpin loop between residues 90 to 103 of monomer 1 (Fig. 2A).
22. J. Stubbe, *Adv. Enzymol. Relat. Areas Mol. Biol.* **63**, 349 (1990).
23. _____ and W. A. van der Donk, *Chem. Rev.* **98**, 705 (1998).
24. S. S. Mao *et al.*, *Biochemistry* **31**, 9733 (1992).
25. J. Stubbe, M. Ator, T. Krenitsky, *J. Biol. Chem.* **258**, 1625 (1983).
26. M. Olcott, J. Andersson, B.-M. Sjöberg, *ibid.* **273**, 24853 (1998).
27. No information is available on where in the class III enzyme formate is acting. H atoms are not transferred directly from formate to the substrate, because when [^{3}H]formate is used, ^{3}H is found almost exclusively in water molecules, suggesting that H atoms pass through a protein-based intermediate [(*13*); R. Eliasson *et al.*, *Biochem. Biophys. Res. Commun.* **214**, 28 (1995)].
28. A. L. Persson *et al.*, *J. Biol. Chem.* **272**, 31533 (1997).
29. R. Lenz and B. Giese, *J. Am. Chem. Soc* **119**, 2784 (1997).
30. P. E. M. Siegbahn, *ibid.* **120**, 8417 (1998).
31. The hydroxyl moiety of Tyr^{441} is within hydrogen bonding distance of the 3′-OH of the modeled substrate and could act as a proton donor in the elimination reaction; however it is not completely conserved, being replaced by Thr and Leu in two archaebacterial sequences.
32. Indeed, in the quantum mechanical calculations performed on *E. coli* R1, in which formate was used as a model for Glu^{441}, the lowest energy transition state for the water elimination step was found when formate bridged the 2′-OH and 3′-OH positions (*30*).
33. The side chain of Cys^{290} is hydrogen-bonded to that of Lys^{233}, which is buried in the interior of the protein. Lys^{233} could be important for modulating the properties of Cys^{290}, but this structure does not support its involvement in radical transfer. The carbonyl oxygen of Cys^{579} hydrogen bonds to the side chain of Arg^{291}, and the side chain of Tyr^{581} is directed toward the 2′-C of the modeled substrate. However, the role of this tyrosine in radical transfer is currently unclear, because a mutant of *E. coli* NrdD where it is altered to Phe retains 7% activity (*8*).
34. M. Frey, M. Rothe, A. F. Wagner, J. Knappe, *J. Biol. Chem.* **269**, 12432 (1994).
35. Silver-stained gels of washed and redissolved crystals indicate the presence of NrdG in the crystals. The lack of electron density is probably due to partial occupancy. The affinity of NrdG for NrdD(G580A) may be affected by the integrity of the iron-sulfur-cluster, which we made no special effort to ensure was intact throughout purification and crystallization of the complex.
36. J. Andersson and B.-M. Sjöberg, in preparation. The most likely position for these residues in the current structure is in the relatively disordered structure near the end of strand βJ, and a large conformational change would be required to bring them to a position near Gly^{580}.
37. J. Knappe and A. F. Wagner, *Methods Enzymol.* **258**, 343 (1995).
38. A. F. Wagner, M. Frey, F. A. Neugebauer, W. Schafer, J. Knappe, *Proc. Natl. Acad. Sci. U.S.A.* **89**, 996 (1992).
39. J. B. Broderick *et al.*, *J. Am. Chem. Soc.* **119**, 7396 (1997).
40. R. Külzer, T. Pils, R. Kappl, J. Huttermann, J. Knappe, *J. Biol. Chem.* **273**, 4897 (1998).
41. X. Sun *et al.*, *Proc. Natl. Acad. Sci. U.S.A.* **90**, 577 (1993).
42. The 10 residues between amino acids 275 and 284 that are missing in PFL and in the *Methanococcus jannaschii* class III RNR correspond to helix αE and a short loop, both on the side of the barrel distal from the active site. These could presumably be lost during evolution without affecting the structural integrity.
43. C. V. Parast *et al.*, *Biochemistry* **34**, 2393 (1995); S. G. Reddy *et al.*, *ibid.* **37**, 558 (1998).
44. E. Mulliez, M. Fontecave, J. Gaillard, P. Reichard, *J. Biol. Chem.* **268**, 2296 (1993).
45. Reviewed in G. Sawers and G. Watson, *Mol. Microbiol.* **29**, 945 (1998).
46. Z. Otwinowski and W. Minor, *Methods Enzymol.* **276**, 307 (1997).
47. Collaborative Computational Project No. 4, *Acta Crystallogr.* **D50**, 760 (1994).
48. For data collection, crystals were soaked in crystal mother liquor containing ~45% PEG 400 instead of the 28 to 32% in which they were grown, and flash-cooled to 77 K in liquid nitrogen. $MgCl_2$ was removed from the mother liquor for the nucleotide soaks because it caused precipitation of the nucleotides in the presence of PEG. The presence of Os and Hg in the crystals was determined at the time of data collection by x-ray fluorescence spectroscopy. Sites in MMA and KOs were found independently by anomalous difference Pattersons, although they turned out to have four common sites; IrCl was solved by difference Fourier with phases from the first two, but was poorly substituted. All Hg and some of the Os sites are covalently linked to free Cys residues and were used as markers during model building. Heavy-atom parameter refinement and phasing was carried out with MLPHARE [Z. Otwinowski, *Proceedings of the CCP4 Study Weekend* (Science and Engineering Research Council, Daresbury Laboratory, Warrington, UK, 1991), p. 80]. To minimize bias, only one set of isomorphous differences was refined for each derivative; for the other wavelengths, anomalous differences only were used [D. T. Logan, M.-H. Mazauric, D. Kern, D. Moras, *EMBO J.* **14**, 4156 (1995)]. The hand of the space group and of the anomalous differences was determined by inspecting electron density maps solvent-flattened with DM [K. Cowtan, *Joint CCP4 ESF-EACBM Newslett. Protein Crystallogr.* **31**, 34 (1994)] for interpretability. Solvent flattening improved the mean figure of merit from 0.61 to 0.74. Despite the weak anomalous signals and common sites, over 300 residues of poly-Ser model could be built into these maps, which was refined with the program TNT [D. E. Tronrud, L. F. ten Eyck, B. W. Matthews, *Acta Crystallogr.* **D53**, 240 (1987)], at first by rigid body refinement, then very tightly restrained atomic refinement. Calculated phases were combined with experimental phases, and maps were subjected to further density modification. Many cycles of such model building and phase improvement were carried out. When all visible side chains had been built, one cycle of torsion angle dynamics [L. M. Rice and A. T. Brünger, *Proteins* **19**, 277 (1994)] was carried out with the program X-PLOR. Further refinement against the second data set was performed with TNT and Refmac [G. N. Murshudov, A. A. Vagin, E. J. Dodson, *Acta Crystallogr.* D53, 240 (1997)].
49. A. L. Morris, M. W. MacArthur, E. G. Hutchinson, J. M. Thornton, *Proteins* **12**, 345 (1992).
50. All figures were made using the programs Molscript [P. J. Kraulis, *J. Appl. Crystallogr.* **24**, 946 (1991)], Bobscript [R. M. Esnouf, *J. Mol. Graphics Modelling* **15**, 132 (1997)], and Raster3D [E. A. Merritt and M. J. Murphy, *Acta Crystallogr.* **D50**, 869 (1994)].

51. We acknowledge the contributions of P. Young and M. Westman to protein purification, assistance with data collection from V. Stojanoff and A. Thompson (BM14), M. Capel (X12B), K. Knudsen (SNBL), and outstation staff at EMBL, Hamburg. We also thank M. Thunnissen for help with early map interpretation. This work was funded by grants from the Swedish Natural Sciences Research Council to D.L., P.N., and B.-M.S and from the Swedish Cancer Foundation to B.-M.S. It was carried out in part at the NSLS, which is supported by the U.S. Department of Energy, Division of Materials Sciences and Division of Chemical Sciences. The structure of the anaerobic ribonucleotide reductase NrdD subunit has been deposited with the Protein Data Bank (accession number 1B8B).

11 November 1998; accepted 26 January 1999